On the thermodynamic Bethe ansatz equation in the sinh-Gordon model

2006 J. Phys. A: Math. Gen. 39 12863

(http://iopscience.iop.org/0305-4470/39/41/S09)

INSTITUTE OF PHYSICS PUBLISHING JOURNAL OF PHYSICS A: MATHEMATICAL AND GENERAL

J. Phys. A: Math. Gen. **39** (2006) 12863–12887 doi:10.1088/0305-4470/39/41/S09

On the thermodynamic Bethe ansatz equation in the sinh-Gordon model

Al Zamolodchikov[1]

Laboratoire de Physique Théorique et Astroparticules[2], Université Montpellier II, Pl.E.Bataillon, 34095 Montpellier, France

Received 8 February 2006, in final form 16 July 2006
Published 27 September 2006
Online at stacks.iop.org/JPhysA/39/12863

Abstract

Two implicit periodic structures in the solution of the sinh-Gordon thermodynamic Bethe ansatz (TBA) equation are considered. The analytic structure of the solution as a function of complex θ is studied to some extent both analytically and numerically. The results hint at how the CFT integrable structures can be relevant in the sinh-Gordon and staircase models. More motivations are figured out for subsequent studies of the massless sinh-Gordon (i.e. Liouville) TBA equation.

PACS numbers: 02.30.Ik, 05.50.+q, 11.25.Hf

1. Sinh-Gordon model

It seems that from the recent developments of the string theory, there are some persistent requests about a better understanding of the two-dimensional sigma models with non-compact (in particular singular) target spaces. Physical properties of such models are expected to be quite different from those of the better studied compact sigma models. It is therefore a challenge for the two-dimensional integrable field theory community to reveal the corresponding peculiarities and new features.

The two-dimensional sinh-Gordon model (ShG) is defined by the (Euclidean) action

$$A_{\mathrm{ShG}} = \int \left[\frac{1}{4\pi} (\partial_a \phi)^2 + 2\mu \cosh(2b\phi) \right] \mathrm{d}^2 x. \tag{1.1}$$

I believe that this model can be considered as 'a model' of (suitably perturbed) non-compact sigma models in the sense that its properties are considerably different from those of the perturbed rational conformal field theories, these differences being sometimes quite similar to those between non-compact and compact sigma models.

[1] On leave of absence from Institute of Theoretical and Experimental Physics, B. Cheremushkinskaya 25, 117259 Moscow, Russia.
[2] Laboratoire Associé au CNRS UMR-5207.

In (1.1), μ is a dimensional (of dimension $\mu \sim [\text{mass}]^{2+2b^2}$) coupling constant which determines the scale in the model and b is the dimensionless ShG parameter. For the beginning I suppose it to be real and non-negative. The case $b = 0$ turns to be somewhat singular for the subsequent considerations, and here the study is restricted to positive values $0 < b < \infty$ only. It is also convenient to use different parameters

$$Q = b + 1/b \tag{1.2}$$

and

$$p = \frac{b}{Q} = \frac{b^2}{1+b^2} \tag{1.3}$$

instead of b.

The perturbing operators $\exp(\pm 2b\phi)$ in (1.1) have negative dimension $\Delta = -b^2$. To make the coupling μ a strict sense, we need to fix a normalization of these operators. Here, they are implied to be normal ordered w.r.t. the massless (unperturbed) vacuum in the way that in the unperturbed theory

$$\left\langle \mathrm{e}^{2b\varphi(x_1)} \dots \mathrm{e}^{2b\varphi(x_n)}\, \mathrm{e}^{-2b\varphi(y_1)} \dots \mathrm{e}^{-2b\varphi(y_n)} \right\rangle_{\mu=0} = \frac{\prod_{i,j} |x_i - y_j|^{4b^2}}{\prod_{i>j} (|x_i - x_j||y_i - y_j|)^{4b^2}}. \tag{1.4}$$

The model is known to be integrable and can be solved for many important characteristics. In particular, its factorized scattering theory is known since long [1, 2]. The spectrum consists of only one neutral particle $B(\theta)$ subject to a factorized scattering with two-particle amplitude:

$$S(\theta) = \frac{\sinh\theta - \mathrm{i}\sin\pi p}{\sinh\theta + \mathrm{i}\sin\pi p}, \tag{1.5}$$

With the normalization (1.4), the mass m of this particle is related to the scale parameter μ as [3]

$$\pi\mu \frac{\Gamma(b^2)}{\Gamma(1-b^2)} = [mZ(p)]^{2+2b^2}, \tag{1.6}$$

where

$$Z(p) = \frac{1}{8\sqrt{\pi}} p^p (1-p)^{1-p} \Gamma\left(\frac{1-p}{2}\right) \Gamma\left(\frac{p}{2}\right). \tag{1.7}$$

Note that the scattering theory is invariant under the (weak–strong coupling) duality transformation $b \to 1/b$ which brings $p \to 1-p$. This means that the physical content of the model remains unchanged up to the overall mass scale. Since the combination (1.7) is again invariant under $p \to 1-p$, the mass scale also remains unchanged if the coupling constant μ is simultaneously substituted by the 'dual' coupling constant $\tilde{\mu}$ related to μ as follows:

$$\left(\pi\mu \frac{\Gamma(b^2)}{\Gamma(1-b^2)}\right)^{1/b} = \left(\pi\tilde{\mu} \frac{\Gamma(1/b^2)}{\Gamma(1-1/b^2)}\right)^{b}. \tag{1.8}$$

Therefore, the sinh-Gordon model is completely invariant under the duality $b \to 1/b$; $\mu \to \tilde{\mu}$. Due to this symmetry, it is sufficient to consider only the region $0 < b^2 \leqslant 1$ or $0 < p \leqslant 1/2$.

The infinite volume bulk vacuum energy of the model is also known exactly [4]. In terms of the particle mass m, it is given by the following apparently self-dual expression:

$$\mathcal{E} = \frac{m^2}{8\sinh\pi p}. \tag{1.9}$$

2. TBA equation

In contrast to the on-mass-shell data of ShG quoted above, the off-mass-shell characteristics such as the correlation functions (with the exception of the vacuum expectation values of some local fields [5, 6] and their matrix elements between the asymptotic states [7]) are not known exactly.

Some progress can be made for the finite size effects where the problem is reduced to a nonlinear integral equation known as the thermodynamic Bethe ansatz (TBA) equation. Namely, consider the ground state energy $E(R)$ of the finite-size ShG model placed on a circle of finite circumference R. In the TBA framework, it appears as

$$E(R) = -\frac{m}{2\pi}\int \cosh\theta \log(1+\mathrm{e}^{-\varepsilon(\theta)})\,\mathrm{d}\theta. \tag{2.1}$$

It is convenient to introduce also the R-dependent effective central charge $c_{\mathrm{eff}}(R)$ as

$$c_{\mathrm{eff}}(R) = -\frac{6R}{\pi}E(R). \tag{2.2}$$

In (2.1), $\varepsilon(\theta)$ is the solution of the TBA equation

$$mR\cosh\theta = \varepsilon + \varphi * \log(1+\mathrm{e}^{-\varepsilon(\theta)}), \tag{2.3}$$

where $*$ denotes the θ convolution. The kernel $\varphi(\theta)$ is related to the ShG scattering data (1.5):

$$\varphi(\theta) = -\frac{\mathrm{i}}{2\pi}\frac{\mathrm{d}}{\mathrm{d}\theta}\log S(\theta) = \frac{1}{2\pi}\frac{4\sin\pi p\cosh\theta}{\cosh 2\theta - \cos 2\pi p}. \tag{2.4}$$

The Fourier transform of the kernel reads

$$\varphi(\omega) = \int \mathrm{e}^{\mathrm{i}\omega\theta}\varphi(\theta)\,\mathrm{d}\theta = \frac{\cosh(a\pi\omega/2)}{\cosh(\pi\omega/2)}, \tag{2.5}$$

where the parameter

$$a = 1-2p \tag{2.6}$$

is simply reflected $a \to -a$ under the dualily $p \to 1-p$ and therefore can be taken non-negative $0 \leqslant a < 1$.

The following conclusion is readily made from the structure of the integral equation (2.3).

(i) Function $\varepsilon(\theta)$ is even $\varepsilon(\theta) = \varepsilon(-\theta)$ and analytic in the strip $|\mathrm{Im}\,\theta| < \pi/2 - \pi a/2$. At $\mathrm{Re}\,\theta \to \infty$ in this strip, it has the asymptotic $\varepsilon(\theta) \sim m\,\mathrm{R}\,\mathrm{e}^{\theta}/2$. Therefore, the function

$$Y(\theta) = \exp(-\varepsilon(\theta)) \tag{2.7}$$

is analytic and non-zero in this strip and at $\mathrm{Re}\,\theta \to \infty$ behaves as

$$Y(\theta) \sim \exp(-m\,\mathrm{R}\,\mathrm{e}^{\theta}/2). \tag{2.8}$$

The asymptotic at $\mathrm{Re}\,\theta \to -\infty$ is related to (2.8) by the symmetry $Y(\theta) = Y(-\theta)$. Let us define another even function

$$X(\theta) = \exp\left[-\frac{mR}{2\sin\pi p}\cosh\theta + \int \frac{\log(1+Y(\theta'))}{\cosh(\theta-\theta')}\frac{\mathrm{d}\theta'}{2\pi}\right], \tag{2.9}$$

which is obviously analytic and non-zero in the strip $|\mathrm{Im}\,\theta| < \pi/2$ and at $\mathrm{Re}\,\theta \to \infty$ in this strip

$$X(\theta) \sim \exp\left(-\frac{mR}{4\sin\pi p}\exp\theta\right). \tag{2.10}$$

From the TBA equation, it follows that

$$X(\theta + \mathrm{i}a\pi/2)X(\theta - \mathrm{i}a\pi/2) = Y(\theta). \tag{2.11}$$

(ii) In fact on the real axis, $Y(\theta)$ is real and positive and therefore we expect a strip $|\mathrm{Im}\,\theta| < \epsilon$ with some finite $\epsilon > 0$ where $1 + Y(\theta) \neq 0$. Therefore, the analyticity condition for $X(\theta)$ can be extended to the strip $|\mathrm{Im}\,\theta| < \pi/2 + \epsilon$. This is enough to prove the relation

$$X(\theta + \mathrm{i}\pi/2)X(\theta - \mathrm{i}\pi/2) = 1 + Y(\theta). \tag{2.12}$$

The functional equation

$$X(\theta + \mathrm{i}\pi/2)X(\theta - \mathrm{i}\pi/2) = 1 + X(\theta + \mathrm{i}a\pi/2)X(\theta - \mathrm{i}a\pi/2) \tag{2.13}$$

follows. This relation allows us to extend the original analyticity strip $|\mathrm{Im}\,\theta| < \pi/2 + \epsilon$ to the strip $|\mathrm{Im}\,\theta| < 3\pi/2$ and, as we will see before long, to the whole complex plane of θ so that $X(\theta)$ is an entire function of θ. Note that from (2.13) it follows that the asymptotic (2.10) holds in the larger strip $|\mathrm{Im}\,\theta| < \pi$. The asymptotic outside this strip is more complicated.

(iii) As a consequence, $Y(\theta)$ is also an entire function of θ and satisfies the following functional relation:

$$Y(\theta + \mathrm{i}\pi/2)Y(\theta - \mathrm{i}\pi/2) = (1 + Y(\theta + \mathrm{i}a\pi/2))(1 + Y(\theta - \mathrm{i}a\pi/2)). \tag{2.14}$$

The last equation is very similar to the functional relations appearing in the TBA study of the integrable perturbed rational conformal field theories (the so-called Y systems). Typically, such Y systems imply a periodicity of Y functions in θ with some imaginary period related to the scale dimension Δ of the perturbing operator (see e.g. [8, 9]). This periodicity in order entails a special 'perturbative' structure of the short distance $R \to 0$ behaviour of the ground state energy $E(R)$. Namely, up to one exceptional term, it is a regular expansion in powers of $R^{2-2\Delta}$:

$$E(R) = -\mathcal{E}_{\mathrm{vac}} R - \frac{\pi}{6R} \sum_{n=0}^{\infty} c_n R^{(2-2\Delta)n}, \qquad R \to 0, \tag{2.15}$$

where $\mathcal{E}_{\mathrm{vac}}$ is the infinite volume vacuum energy of the model. Unlike this typical situation, the Y system (2.14) (or the X system (2.13)) does not imply any apparent periodic structure of $Y(\theta)$ in θ. As a manifestation of this peculiarity, the $R \to 0$ behaviour of $E(R)$ is different from (2.15) and includes softer logarithmic corrections [10]:

$$E(R) = -\mathcal{E} R - \frac{\pi}{6R}\left(1 - \frac{3\pi^2 p(1-p)}{2\log^2 R} + O(\log^{-3} R)\right), \qquad R \to 0. \tag{2.16}$$

The purpose of the following two sections is to reveal two hidden periodic structures (with different periods) of the Y system (2.14).

3. Discrete Liouville equation

In this section, I discuss the following two-dimensional nonlinear finite-difference equation for the function $X(u, v)$:

$$X(u+1, v)X(u-1, v) = 1 + X(u, v+1)X(u, v-1), \tag{3.1}$$

which is apparently resemblant of the functional X system (2.13). In the following section, we will see how some of the results for (3.1) can be specialized to our TBA problem. Equation (3.1) is a particular case of a Hirota difference equation [11]. The constructions of this section can be found in [12] (see also [13]) where a more general difference system is analysed. They also appeared in a quite close context in [14].

Equation (3.1) can be considered as a discretization of the hyperbolic Liouville equation

$$\partial_u^2 \varphi - \partial_v^2 \varphi = -\mathrm{e}^{2\varphi}. \tag{3.2}$$

Indeed, let $X(u,v) = \exp(-\varphi(u,v))$ and let $\varphi(u,v)$ be large and negative. Then, equation (3.1) is approximated by

$$\varphi(u+1,v)+\varphi(u-1,v)-\varphi(u,v+1)-\varphi(u,v-1) = -\exp(\varphi(u,v+1)+\varphi(u,v-1)). \tag{3.3}$$

In the long-wave limit, this is reduced to (3.2). As we will see below, equation (3.1) is in many respects very similar to the Liouville equation. It seems quite natural to call it the discrete Liouville equation [15].

Let me recall the well-known construction of a local solution to equation (3.2).

(1a) It is convenient to use the light cone variables $x^+ = u+v$ and $x^- = u-v$ so that $\partial_+ = (\partial_u+\partial_v)/2$, $\partial_- = (\partial_u-\partial_v)/2$ and (3.2) reads

$$4\partial_+\partial_-\varphi = -\mathrm{e}^{2\varphi}. \tag{3.4}$$

Let φ be a local solution of (3.4). Define

$$t = -(\partial_+\varphi)^2+\partial_+^2\varphi, \qquad \tilde{t} = -(\partial_-\varphi)^2+\partial_-^2\varphi. \tag{3.5}$$

As a consequence of equation (3.4), we have

$$\partial_- t = \partial_+\tilde{t} = 0 \tag{3.6}$$

so that $t(x^+)$ and $\tilde{t}(x^-)$ are respectively functions of only x^+ and x^-.

(2a) The field $X = \exp(-\varphi)$ satisfies two linear differential equations:

$$\big(\partial_+^2+t(x^+)\big)X(u,v) = 0, \qquad \big(\partial_-^2+\tilde{t}(x^-)\big)X(u,v) = 0. \tag{3.7}$$

(3a) Let $Q_\pm(x)$ and $\tilde{Q}_\pm(x)$ be linearly independent solutions to the ordinary differential equations

$$\big(\partial_x^2+t(x)\big)Q_\pm(x) = 0, \qquad \big(\partial_x^2+\tilde{t}(x)\big)\tilde{Q}_\pm(x) = 0, \tag{3.8}$$

where the coefficient functions $t(x)$ and $\tilde{t}(x)$ are determined by equation (3.5). Suppose these solutions are normalized in the way that

$$\begin{aligned} &\partial_x Q_+(x)Q_-(x)-Q_+(x)\partial_x Q_-(x) = 1/2,\\ &\partial_x \tilde{Q}_+(x)\tilde{Q}_-(x)-\tilde{Q}_+(x)\partial_x \tilde{Q}_-(x) = 1/2. \end{aligned} \tag{3.9}$$

A local solution of (3.4) can be constructed as

$$\exp(-\varphi(u,v)) = Q_+(x^+)\tilde{Q}_+(x^-)+Q_-(x^+)\tilde{Q}_-(x^-). \tag{3.10}$$

(4a) Introduce the functions

$$F(x) = \frac{Q_+(x)}{Q_-(x)}, \qquad G(x) = -\frac{\tilde{Q}_-(x)}{\tilde{Q}_+(x)}. \tag{3.11}$$

The solution (3.10) can be rewritten as

$$\exp 2\varphi(u,v) = \frac{4F'(x^+)G'(x^-)}{(F(x^+)-G(x^-))^2}. \tag{3.12}$$

Note also that in terms of F and G

$$t(x) = -2\{F(x),x\}, \qquad \tilde{t}(x) = -2\{G(x),x\}, \tag{3.13}$$

where

$$\{f(x),x\} = \frac{f'''}{f'}-\frac{3}{2}\left(\frac{f''}{f'}\right)^2 \tag{3.14}$$

is the Schwarz derivative.

Now let us turn to the discrete Liouville equation (3.1). Defining, similar to equation (2.11),

$$Y(u,v) = X(u,v+1)X(u,v-1), \qquad 1+Y(u,v) = X(u+1,v)X(u-1,v), \tag{3.15}$$

we arrive at the finite-difference equation analogous to (2.14):

$$Y(u+1,v)Y(u-1,v) = (1+Y(u,v+1))(1+Y(u,v-1)). \tag{3.16}$$

(1b) Introduce

$$\begin{aligned} T(u,v) &= \frac{X(u+1,v+1)+X(u-1,v-1)}{X(u,v)}, \\ \tilde{T}(u,v) &= \frac{X(u+1,v-1)+X(u-1,v+1)}{X(u,v)}. \end{aligned} \tag{3.17}$$

As a consequence of equation (3.1), we obtain

$$T(u+1,v-1) = T(u,v), \qquad \tilde{T}(u+1,v+1) = \tilde{T}(u,v) \tag{3.18}$$

so that $T = T(u+v)$ and $\tilde{T} = \tilde{T}(u-v)$. In the continuous limit, these objects are related to (3.5) as $T(u) = 2 - 4t(u) + \cdots$ and $\tilde{T}(u) = 2 - 4\tilde{t}(u) + \cdots$ [14].

(2b) Equation (3.17) can be rewritten as (similar to (3.7))

$$\begin{aligned} X(u+1,v+1)+X(u-1,v-1) &= T(u+v)X(u,v), \\ X(u+1,v-1)+X(u-1,v+1) &= \tilde{T}(u-v)X(u,v). \end{aligned} \tag{3.19}$$

(3b) Let $Q_\pm(u)$ and $\tilde{Q}_\pm(u)$ be linearly independent solutions of the second-order finite-difference equations

$$\begin{aligned} Q_\pm(u+2)+Q_\pm(u-2) &= T(u)Q_\pm(u), \\ \tilde{Q}_\pm(u+2)+\tilde{Q}_\pm(u-2) &= \tilde{T}(u)\tilde{Q}_\pm(u), \end{aligned} \tag{3.20}$$

normalized by the 'quantum Wronskians'

$$\begin{aligned} Q_+(u+1)Q_-(u-1) - Q_+(u-1)Q_-(u+1) &= 1, \\ \tilde{Q}_+(u+1)\tilde{Q}_-(u-1) - \tilde{Q}_+(u-1)\tilde{Q}_-(u+1) &= 1. \end{aligned} \tag{3.21}$$

Then, it is verified that

$$X(u,v) = Q_+(u+v)\tilde{Q}_+(u-v) + Q_-(u+v)\tilde{Q}_-(u-v) \tag{3.22}$$

is a local solution of the discrete Liouville equation (3.1).

(4b) Introduce the functions

$$F(u) = \frac{Q_+(u)}{Q_-(u)}, \qquad G(u) = -\frac{\tilde{Q}_-(u)}{\tilde{Q}_+(u)}, \tag{3.23}$$

which can be used to present the local solution (3.22) in the form

$$\begin{aligned} Y(u,v) &= \frac{(F(u+v+1)-G(u-v-1))(F(u+v-1)-G(u-v+1))}{(F(u+v+1)-F(u+v-1))(G(u-v+1)-G(u-v-1))}, \\ 1+Y(u,v) &= \frac{(F(u+v+1)-G(u-v+1))(F(u+v-1)-G(u-v-1))}{(F(u+v+1)-F(u+v-1))(G(u-v+1)-G(u-v-1))}. \end{aligned} \tag{3.24}$$

Let me also mention the discrete analogue of the Schwarz derivative (3.13):

$$T(u+1)T(u-1) = \frac{(F(u+3)-F(u-1))(F(u+1)-F(u-3))}{(F(u+3)-F(u+1))(F(u-1)-F(u-3))}. \tag{3.25}$$

4. Application to TBA

The above constructions for the discrete Liouville equation can be translated for the ShG X system (2.13) we are interested in. Let us require the following periodicity condition for $X(u, v)$ in (3.1):

$$X(u + a, v + 1) = X(u, v), \tag{4.1}$$

with some parameter a (at this point, we start to diverge from the lines of [14]). With this periodicity, equation (3.1) reads

$$X(u + 1, v)X(u - 1, v) = 1 + X(u + a, v)X(u - a, v). \tag{4.2}$$

Here, v can be considered as a parameter. Suppressing this redundant dependence and rescaling u as

$$\theta = \mathrm{i}\pi u/2, \tag{4.3}$$

we are back to the ShG X system in the form (2.13).

From $X(\theta)$, the two functions $T(\theta)$ and $\tilde{T}(\theta)$ are readily restored as

$$\begin{aligned} T(\theta) &= \frac{X(\theta + \mathrm{i}\pi(1 - a)/2) + X(\theta - \mathrm{i}\pi(1 - a)/2)}{X(\theta)}, \\ \tilde{T}(\theta) &= \frac{X(\theta + \mathrm{i}\pi(1 + a)/2) + X(\theta - \mathrm{i}\pi(1 + a)/2)}{X(\theta)}. \end{aligned} \tag{4.4}$$

The 'holomorphic' property (3.18) is translated to the following periodicity of these functions:

$$T(\theta + \mathrm{i}\pi(1 + a)/2) = T(\theta), \qquad \tilde{T}(\theta + \mathrm{i}\pi(1 - a)/2) = \tilde{T}(\theta). \tag{4.5}$$

Note that the period $\mathrm{i}\pi/(1 + b^2)$ of T corresponds to the negative dimension $\Delta = -b^2$ of the perturbing operator in (1.1). As can be anticipated from the self-duality of ShG, the second period $\mathrm{i}\pi b^2/(1 + b^2)$ of $\tilde{T}$ is related to the dimension $\tilde{\Delta} = -b^{-2}$ of the 'dual' exponentials $\exp(\pm 2\phi/b)$.

As is discussed in section 2, $X(\theta)$ is analytic and non-zero in the strip $|\mathrm{Im}\,\theta| < \pi/2$ and analytic in the larger strip $|\mathrm{Im}\,\theta| < 3\pi/2$. Therefore, $T(\theta)$ and $\tilde{T}(\theta)$ are analytic in the strip $|\mathrm{Im}\,\theta| < \pi/2$ and by periodicity (4.5) they are entire functions of θ. It follows from (4.4) that $X(\theta)$ is an entire function of θ too.

The asymptotics at $\mathrm{Re}\,\theta \to \infty$ follow from (2.10) and (4.4):

$$\begin{aligned} T(\theta) &\sim \exp\left(\frac{mR\exp(\theta - \mathrm{i}\pi(1 - p)/2)}{4\cos(\pi p/2)}\right) && \text{in the strip} \quad 0 < \mathrm{Im}\,\theta < \pi(1 + a)/2, \\ \tilde{T}(\theta) &\sim \exp\left(\frac{mR\exp(\theta - \mathrm{i}\pi p/2)}{4\sin(\pi p/2)}\right) && \text{in the strip} \quad 0 < \mathrm{Im}\,\theta < \pi(1 - a)/2. \end{aligned} \tag{4.6}$$

The real axis $\mathrm{Im}\,\theta = 0$ is a Stokes line and here

$$\begin{aligned} T(\theta) &\sim 2\exp\left(\frac{mR}{4}\tan(\pi p/2)\,\mathrm{e}^{\theta}\right)\cos\left(\frac{mR}{4}\exp\theta\right), \\ \tilde{T}(\theta) &\sim 2\exp\left(\frac{mR}{4}\cot(\pi p/2)\,\mathrm{e}^{\theta}\right)\cos\left(\frac{mR}{4}\exp\theta\right). \end{aligned} \tag{4.7}$$

The $\mathrm{Re}\,\theta \to \infty$ asymptotic in the whole plane of θ is restored from periodicity (4.5). Following (4.7) both T and $\tilde{T}$ have an infinite number of zeros on the real axis located at $\theta = \pm\theta_n, n = 1, 2, \ldots, \infty$, with $\theta_n \sim \log(2\pi n/mR) + O(1/n)$ at $n \to \infty$. The half-period

shifted functions $T(\theta + i\pi(1-p)/2)$ and $\tilde{T}(\theta + i\pi p/2)$ are also real at real θ, and at $\theta \to \infty$ they behave as

$$\begin{aligned} T(\theta + i\pi(1-p)/2) &\sim \exp\left(\frac{mR}{4\cos(\pi p/2)}\, e^{\theta}\right), \\ \tilde{T}(\theta + i\pi p/2) &\sim \exp\left(\frac{mR}{4\sin(\pi p/2)}\, e^{\theta}\right). \end{aligned} \tag{4.8}$$

Analytic properties of T and $\tilde{T}$ allow the following convergent expansions:

$$T(\theta) = \sum_{-\infty}^{\infty} T_n \exp(2nQb\theta), \qquad \tilde{T}(\theta) = \sum_{-\infty}^{\infty} \tilde{T}_n \exp(2nQ\theta/b), \tag{4.9}$$

with real T_n and $\tilde{T}_n$. From the symmetry of the original TBA equations, T and $\tilde{T}$ are both even functions of θ, so in our present case $T_n = T_{-n}$ and $\tilde{T}_n = \tilde{T}_{-n}$. These coefficients are the Fourier components of the functions $T(\theta)$ and $\tilde{T}(\theta)$:

$$T_n = \int_{\uparrow} T(\theta) \exp(-2nQb\theta) \frac{bQ\, d\theta}{i\pi}, \qquad \tilde{T}_n = \int_{\uparrow} \tilde{T}(\theta) \exp(-2nQ\theta/b) \frac{Q\, d\theta}{i\pi b}. \tag{4.10}$$

The integrals here are over the periods $i\pi/(Qb)$ and $i\pi b/Q$ of $T(\theta)$ and $\tilde{T}(\theta)$, respectively. The saddle-point approximations for these integrals allow us to read off the leading large n behaviour of the coefficients T_n and $\tilde{T}_n$ from the asymptotics (4.6):

$$\begin{aligned} T_n &\sim (-)^n \sqrt{\frac{bQ}{\pi}}\, n^{-2Qbn-1/2} \left(e \frac{mR}{8\pi bQ\cos(\pi p/2)}\right)^{2Qbn}, \\ \tilde{T}_n &\sim (-)^n \sqrt{\frac{Q}{\pi b}}\, n^{-2Qn/b-1/2} \left(e \frac{bmR}{8\pi Q\sin(\pi p/2)}\right)^{2Qn/b}. \end{aligned} \tag{4.11}$$

So far the constructions were explicitly based on the integral equation (2.3). The rest of the section is more speculative. Suppose that for $T(\theta)$ and $\tilde{T}(\theta)$ constructed as in (4.4), we can find $Q_{\pm}(\theta)$ and $\tilde{Q}_{\pm}(\theta)$, which solve

$$\begin{aligned} Q_{\pm}(\theta + i\pi) + Q_{\pm}(\theta - i\pi) &= T(\theta) Q_{\pm}(\theta), \\ \tilde{Q}_{\pm}(\theta + i\pi) + \tilde{Q}_{\pm}(\theta - i\pi) &= \tilde{T}(\theta) \tilde{Q}_{\pm}(\theta), \end{aligned} \tag{4.12}$$

and are the 'Bloch waves' with respect to the periods of T and $\tilde{T}$, respectively,

$$\begin{aligned} Q_{\pm}(\theta + i\pi(1+a)/2) &= \exp(\pm 2i\pi P/Q) Q_{\pm}(\theta), \\ \tilde{Q}_{\pm}(\theta + i\pi(1-a)/2) &= \exp(\pm 2i\pi P/Q) \tilde{Q}_{\pm}(\theta), \end{aligned} \tag{4.13}$$

with some Floquet index P. Let these be normalized by the quantum Wronskians

$$\begin{aligned} Q_{+}(\theta + i\pi/2) Q_{-}(\theta - i\pi/2) - Q_{+}(\theta - i\pi/2) Q_{-}(\theta + i\pi/2) &= 1, \\ \tilde{Q}_{+}(\theta + i\pi/2) \tilde{Q}_{-}(\theta - i\pi/2) - \tilde{Q}_{+}(\theta - i\pi/2) \tilde{Q}_{-}(\theta + i\pi/2) &= 1. \end{aligned} \tag{4.14}$$

Then formally,

$$X(\theta) = Q_{+}(\theta)\tilde{Q}_{+}(\theta) + Q_{-}(\theta)\tilde{Q}_{-}(\theta) \tag{4.15}$$

solves equation (4.4) as well as the X system (2.13).

Unfortunately, at present I know no effective means to construct these Q functions. Moreover, there are serious doubts that the objects satisfying both (4.12) and (4.13) can be constructed in any sense, at least at rational values of b^2. I hope to say something more definite on this point in the near future.

5. Large Re θ asymptotics

Let me comment a little more about the $\mathrm{Re}\,\theta \to \infty$ asymptotics (with $\mathrm{Im}\,\theta$ fixed) of the function $X(\theta)$ in the whole complex plane. In principle, it can be restored from asymptotic (2.10) in the strip $|\mathrm{Im}\,\theta| \leqslant \pi/2$ using the functional relation (2.13) or, more conveniently, relations (4.4) together with asymptotics (4.6). The asymptotics is always of the form

$$X(\theta) \sim \exp(A(\mathrm{Im}\,\theta)\exp(\mathrm{Re}\,\theta)), \tag{5.1}$$

with some complex function $A(\eta)$ of the real variable $\eta = \mathrm{Im}\,\theta$. Apparently, $\mathrm{Re}\,A(\eta)$ controls the rate of growth of the absolute value of X. At $|\eta| < \pi/2$, we have

$$A(\eta) = -\frac{mR}{4\sin\pi p}\,\mathrm{e}^{\mathrm{i}\eta}. \tag{5.2}$$

It follows from (4.4) that $A(\eta)$ satisfies two functional relations

$$\begin{aligned} A(\eta+\pi(1-a)/2) &= \begin{cases} A(\eta)+\sigma(\eta) & \text{if } \mathrm{Re}(A(\eta)+\sigma(\eta)) > \mathrm{Re}\,A(\eta+\pi(1-a)/2) \\ A(\eta+\pi(1-a)/2) & \text{otherwise} \end{cases} \\ A(\eta+\pi(1+a)/2) &= \begin{cases} A(\eta)+\tilde\sigma(\eta) & \text{if } \mathrm{Re}(A(\eta)+\tilde\sigma(\eta)) > \mathrm{Re}\,A(\eta+\pi(1+a)/2) \\ A(\eta+\pi(1+a)/2) & \text{otherwise,} \end{cases} \end{aligned} \tag{5.3}$$

where the functions $\sigma(\eta)$ and $\tilde\sigma(\eta)$ control the asymptotics of $T(\theta)$ and $\tilde T(\theta)$, respectively. They are defined as

$$\begin{aligned} \sigma(\eta) &= \frac{mR}{4\cos(\pi p/2)}\exp(\mathrm{i}\eta - \mathrm{i}\pi(1-p)/2) \qquad \text{at} \quad 0 \leqslant \eta < (1+a)/2 \\ \tilde\sigma(\eta) &= \frac{mR}{4\sin(\pi p/2)}\exp(\mathrm{i}\eta - \mathrm{i}\pi p/2) \qquad \text{at} \quad 0 \leqslant \eta < (1-a)/2, \end{aligned} \tag{5.4}$$

and continued outside these regions periodically as $\tilde\sigma(\eta + \pi(1-a)/2) = \tilde\sigma(\eta)$ and $\sigma(\eta+\pi(1+a)/2) = \sigma(\eta)$. Both $\sigma(\eta)$ and $\tilde\sigma(\eta)$ jump by $-\mathrm{i}mR/2$ at $\eta = \pi(1+a)n/2$, $n \in Z$, and $\eta = \pi(1+a)n/2$, $n \in Z$, respectively. This corresponds to the limiting density of zeros prescribed by (4.7).

A common solution to (5.3) exists. Generally, the solution is discontinuous at all values $\eta = \pm\pi(m(1+a)/2 + n(1-a)/2)$ with arbitrary positive integers n and m. At each such point, the imaginary part $\mathrm{Im}\,A$ jumps down by $-mR/2$ indicating an asymptotic line of accumulation of zeros of $X(\theta)$, the asymptotic density being the same as that of the functions T and $\tilde T$ (4.7). The real part of A at these points is continuous itself but has discontinuities in the first derivative. The first Stokes line appears at $\eta = \pi$.

At large η, the structure is qualitatively different depending on the arithmetic nature of the parameter b^2. If it is a rational number, the periods of T and $\tilde T$ are commensurable. Some of the discontinuities merge forming multiple jumps in the imaginary part. The solution $A(\theta)$ bears a regular 'quasiperiodic' structure with the common period of T and $\tilde T$. For irrational b^2, the periods are incommensurable and as $\eta \to \infty$ the singularities are more and more dense, the solution having quite irregular behaviour.

In figure 1, the real and imaginary parts of $A(\eta)$ are plotted for the simplest (self-dual) case $b = 1$. Both periods are equal to $\pi/2$. The discontinuities are located at $\eta = \pm\pi(n+1)/2$, $n = 1, 2, \ldots$, where the imaginary part jumps by $-mRn/2$. In contrast to the location of zeros of T, zeros of X cannot lie exactly on the lines $\mathrm{Im}\,\theta = \mathrm{const}$, at least for the first line $\eta = \pi$. Indeed, in the case $b^2 = 1$ it follows from the functional relation that at real θ,

$$|X(\theta + \mathrm{i}\pi)|^2 = X^2(\theta) + T^2(\theta), \tag{5.5}$$

which is strictly positive.

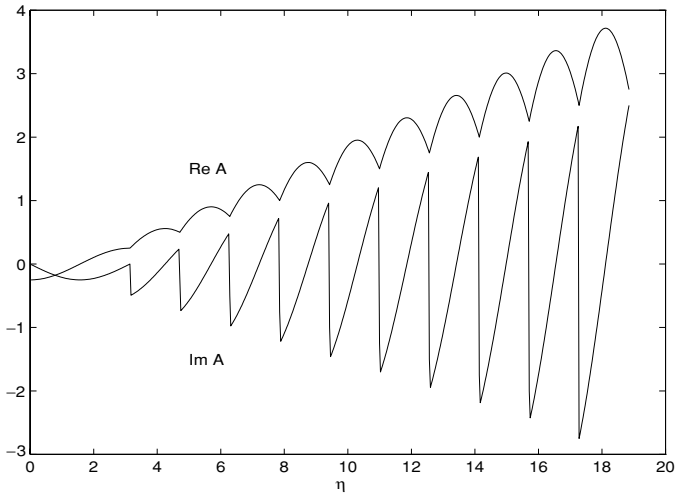

Figure 1. Real and imaginary parts of $A(\eta)/mR$ at $b^2 = 1$.

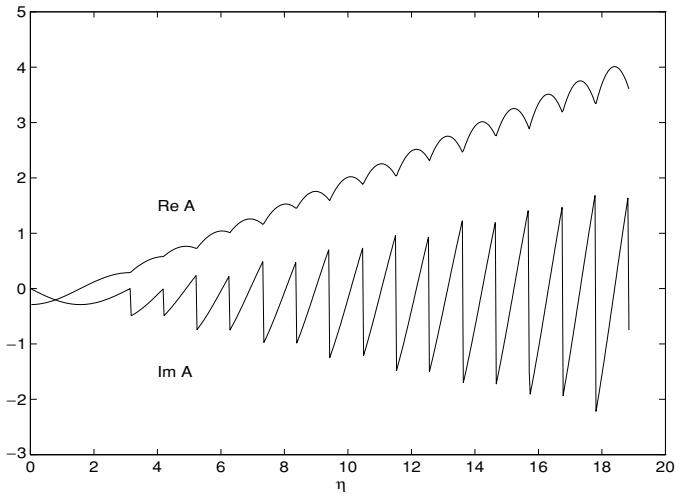

Figure 2. Real and imaginary parts of $A(\eta)/mR$ at $b^2 = 1/2$.

Another rational situation $b^2 = 1/2$ corresponds to the periods $\pi/3$ and $2\pi/3$. The function $A(\eta)$ is plotted in figure 2. The structure is again quite regular, the discontinuities occurring at $\eta = \pi + n\pi/3$, $n = 1, 2, \ldots$, the first two discontinuities in Im A being $-mR/2$, the next two being twice of this amount, then next two being three times, and so on.

With irrational b^2 the picture is far less regular. To illustrate what happens when b^2 slightly deviates from a simple rational number, in figure 3 we plot $A(\eta)$ for $b^2 = 0.8086\ldots$, which is reasonably close to 1. Comparing with figure 1, we see that the first discontinuity at $\eta = \pi$ remains basically the same while the second (double) discontinuity at $\eta = 3\pi/2$ splits into two simple jumps, the third (triple) splits into three simple jumps, and so on. At some point, these splitted groups come to overlap and the picture turns irregular.

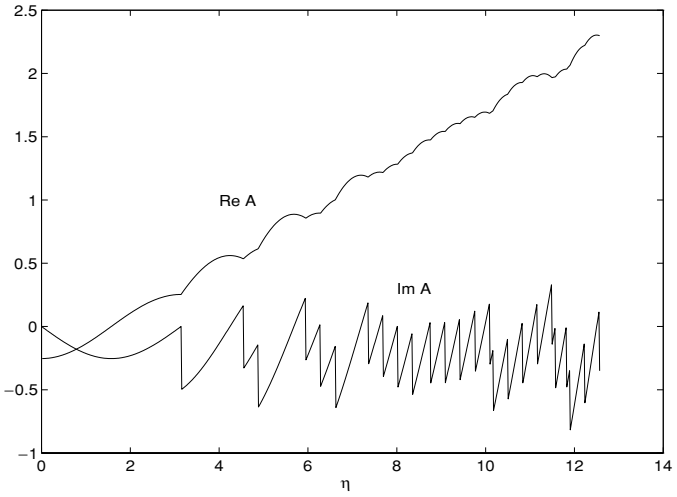

Figure 3. Real and imaginary parts of $A(\eta)/mR$ at $b^2 = 0.8086\ldots$.

6. Staircase situation

The staircase model [10] is a formal analytic continuation of ShG to complex values of the parameter b such that $b^{-1} = b^*$. Although the physical content of this continuation is not completely clear from the field theory point of view, the TBA equation (2.3) remains completely sensible and this continuation of (2.3) can be studied on its own footing. The effective central charge (2.2) is still real and sometimes develops quite intriguing patterns (see [10]).

In [10], the complex b has been parametrized as follows:

$$b^2 = \frac{1 + 2\mathrm{i}\theta_0/\pi}{1 - 2\mathrm{i}\theta_0/\pi}, \tag{6.1}$$

with real $0 \leqslant \theta_0 < \infty$. The parameter p of (1.3) now reads

$$p = \frac{1}{2} + \frac{\mathrm{i}\theta_0}{\pi}, \tag{6.2}$$

while $1 - p = p^*$ and a defined in (2.6) is purely imaginary $a = -2\mathrm{i}\theta_0/\pi$. The TBA kernel (2.4) is real and reads

$$\varphi(\theta) = \frac{1}{2\pi}\left(\frac{1}{\cosh(\theta + \theta_0)} + \frac{1}{\cosh(\theta - \theta_0)}\right), \tag{6.3}$$

with the Fourier transform

$$\varphi(\omega) = \frac{\cos(\omega\theta_0)}{\cosh(\pi\omega/2)}. \tag{6.4}$$

After this substitution the integral equation (2.3) determines real-analytic functions $\varepsilon(\theta)$, $Y(\theta)$ and, through (2.9), real-analytic and symmetric $X(\theta)$ with the asymptotic behaviour at $\mathrm{Re}\,\theta \to \infty$ in the strip $-\pi/2 < \mathrm{Im}\,\theta < \pi/2$:

$$X(\theta) \sim \exp\left(-\frac{mR}{4\cosh\theta_0}\exp\theta\right). \tag{6.5}$$

The functional equation (2.13) now reads

$$X(\theta + \mathrm{i}\pi/2)X(\theta - \mathrm{i}\pi/2) = 1 + X(\theta + \theta_0)X(\theta - \theta_0). \tag{6.6}$$

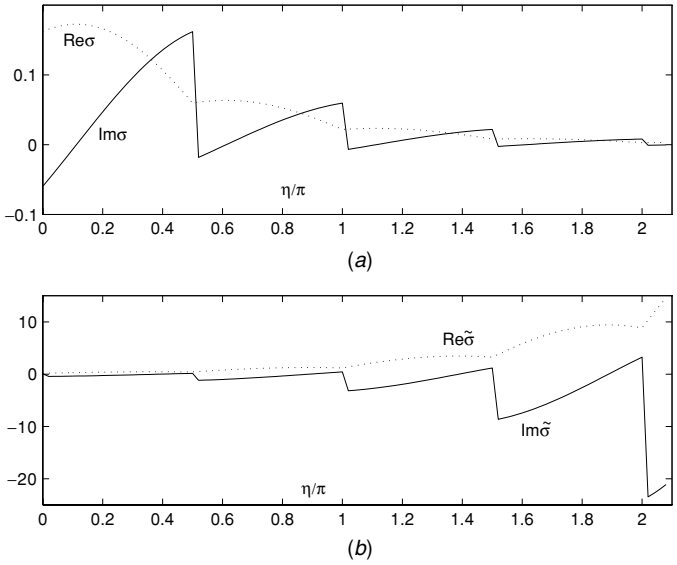

Figure 4. Real and imaginary parts of $\sigma(\eta)/mR$ (a) and $\tilde{\sigma}(\eta)/mR$ (b). The staircase example for $\theta_0 = 1$.

All the considerations of section 4 can be repeated literally. $X(\theta)$ is still an entire function as well as $T(\theta)$ and $\tilde{T}(\theta)$ defined in equation (4.4), and asymptotic (6.5) can be extended to the strip $-\pi < \operatorname{Im}\theta < \pi$. The difference is that the periods of $T(\theta)$ and $\tilde{T}(\theta)$,

$$\begin{aligned} T(\theta+\tau) &= T(\theta), \qquad & \tau &= \mathrm{i}\pi(1+a)/2 = \mathrm{i}\pi/2 + \theta_0, \\ \tilde{T}(\theta+\tilde{\tau}) &= \tilde{T}(\theta), \qquad & \tilde{\tau} &= \mathrm{i}\pi(1-a)/2 = \mathrm{i}\pi/2 - \theta_0, \end{aligned} \tag{6.7}$$

are now complex $\tau = -\tilde{\tau}^*$. The functions $T(\theta) = T(-\theta)$ and $\tilde{T}(\theta) = \tilde{T}(-\theta)$ are still symmetric but no more real analytic. Instead

$$T^*(\theta) = \tilde{T}(\theta^*). \tag{6.8}$$

Expansions similar to (4.9),

$$T(\theta) = \sum_{-\infty}^{\infty} T_n \exp(2\mathrm{i}\pi n\theta/\tau), \qquad \tilde{T}(\theta) = \sum_{-\infty}^{\infty} \tilde{T}_n \exp(2\mathrm{i}\pi n\theta/\tilde{\tau}), \tag{6.9}$$

are convergent and $T_n = T_{-n}$, $\tilde{T}_n = \tilde{T}_{-n}$. Instead of being real as in the real b case, these coefficients are complex conjugate $T_n^* = \tilde{T}_n$.

In the strip $0 < \operatorname{Im}\theta < \pi/2$, the following $\operatorname{Re}\theta \to \infty$ asymptotics hold for T and $\tilde{T}$:

$$\begin{aligned} T(\theta) &\sim X(\theta+\tilde{\tau})/X(\theta) \sim \exp\left(\frac{mR(1-\mathrm{i}\exp(-\theta_0))}{4\cosh\theta_0}\,\mathrm{e}^{\theta}\right), \\ \tilde{T}(\theta) &\sim X(\theta+\tau)/X(\theta) \sim \exp\left(\frac{mR(1-\mathrm{i}\exp(\theta_0))}{4\cosh\theta_0}\,\mathrm{e}^{\theta}\right). \end{aligned} \tag{6.10}$$

The asymptotic changes at the Stokes line along the real axis where

$$\begin{aligned} T(\theta) &\sim 2\exp\left(\frac{mR(1+\mathrm{i}\sinh\theta_0)}{4\cosh\theta_0}\,\mathrm{e}^{\theta}\right)\cos\left(\frac{mR}{4}\,\mathrm{e}^{\theta}\right), \\ \tilde{T}(\theta) &\sim 2\exp\left(\frac{mR(1-\mathrm{i}\sinh\theta_0)}{4\cosh\theta_0}\,\mathrm{e}^{\theta}\right)\cos\left(\frac{mR}{4}\,\mathrm{e}^{\theta}\right), \end{aligned} \tag{6.11}$$

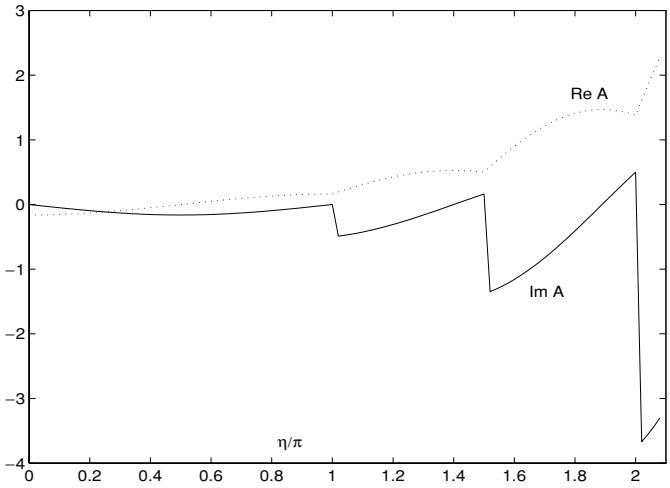

Figure 5. A staircase example of $A(\eta)/mR$ at $\theta_0 = 1$.

and we again observe an infinite sequence of zeros accumulating at infinity, the density being the same as in the real b case of section 5. In the strips $\pi n/2 < \operatorname{Im}\theta < \pi(n+1)/2$ (with an arbitrary integer n), the $\operatorname{Re}\theta \to \infty$ asymptotics follow from periodicity (6.7). In particular, along the lines $\operatorname{Im}\theta = \mathrm{i}n\pi/2$ (with any integer n), we will have

$$\begin{aligned} T(\theta) &\sim 2\exp\left(\frac{mR(1+\mathrm{i}\sinh\theta_0)}{4\cosh\theta_0}\,\mathrm{e}^{\operatorname{Re}\theta - n\theta_0}\right)\cos\left(\frac{mR}{4}\,\mathrm{e}^{\operatorname{Re}\theta-n\theta_0}\right), \\ \tilde{T}(\theta) &\sim 2\exp\left(\frac{mR(1-\mathrm{i}\sinh\theta_0)}{4\cosh\theta_0}\,\mathrm{e}^{\operatorname{Re}\theta + n\theta_0}\right)\cos\left(\frac{mR}{4}\,\mathrm{e}^{\operatorname{Re}\theta+n\theta_0}\right). \end{aligned} \tag{6.12}$$

The functions $\sigma(\eta)$ and $\tilde{\sigma}(\eta)$ which control the asymptotics of T and $\tilde{T}$ at $\operatorname{Re}\theta \to \infty$,

$$T(\theta) \sim \exp(\sigma(\operatorname{Im}\theta)\,\mathrm{e}^{\operatorname{Re}\theta}), \qquad \tilde{T}(\theta) \sim \exp(\tilde{\sigma}(\operatorname{Im}\theta)\,\mathrm{e}^{\operatorname{Re}\theta}), \tag{6.13}$$

are plotted in figure 4 for the case $\theta_0 = 1$. It is enough to present them for $\eta \geqslant 0$ since $\sigma(-\eta) = \tilde{\sigma}^*(\eta)$. The imaginary part of $\sigma(\eta)$ jumps at the points $\eta = n\pi/2$ by the amount $-mR\exp(-n\theta_0)/2$, in accord with the density of zeros predicted by (6.12). Unlike the previously considered case of real b, in the staircase situation the zeros of T and $\tilde{T}$ are not located exactly at the lines $\operatorname{Im}\theta = \mathrm{i}n\pi/2$ but slightly shifted in the imaginary direction (we will observe this deviation numerically in the following section) and approach these lines asymptotically as $\operatorname{Re}\theta \to \infty$.

Note also that $T(\theta)$ is a single-valued function of $\xi = \exp(2\mathrm{i}\pi\theta/\tau)$. In the complex plane of this variable, the asymptotic lines of accumulation of zeros $\operatorname{Im}\theta = 0, \operatorname{Re}\theta \to \pm\infty$ are parts of the spiral $|\xi| = \exp(\pi \arg\xi/2\theta_0)$ near which the zeros become dense at $|\xi| \to \infty$ or $|\xi| \to 0$, the density growing as $|\xi|^{\pm(1/4+\theta_0^2/\pi^2)}$. Therefore, the large (or small) $|\xi|$ asymptotic of $T(\xi)$ at fixed $\arg\xi$ is rather complicated.

The large $\operatorname{Re}\theta$ asymptotic of $X(\theta)$ at fixed $\eta = \operatorname{Im}\theta$ is controlled by the function $A(\eta)$ (see equation (5.1)). An example corresponding to the case $\theta_0 = 1$ is presented in figure 5. At the points $\eta = \pm\pi(n+1)/2$, $n = 1, 2, \ldots$, the imaginary part of $A(\eta)$ has discontinuities equal to $-mR\sinh(n\theta_0)/(2\sinh\theta_0)$. These amounts determine the asymptotic density of zeros of $X(\theta)$ along these lines.

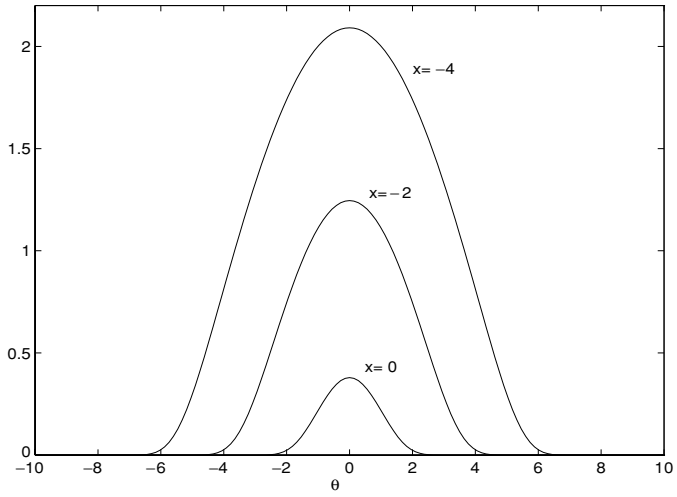

Figure 6. Typical bell-shaped patterns of $X(\theta)$ on the real axis ($b^2 = 1$).

7. Numerics

The integral equation (2.3) can be easily solved numerically e.g. by iterations. The iterations happen to be well convergent (the convergence is somewhat slower if R approaches to 0 or the parameter p is taken to be very small). In the strip $|\mathrm{Im}\,\theta| < \pi/2$, the function $X(\theta)$ can be computed using the integral representation (2.9). This allows us to continue $X(\theta)$ to the whole complex plane iterating relation (2.13) (in fact at large $\mathrm{Im}\,\theta$ it is more convenient to first evaluate $T(\theta)$ inside its period and then use (4.4)). In the rest of this section, we will use the logarithmic scale parameter $x = \log(mR/2)$ instead of R.

7.1. Self-dual point $b^2 = 1$

In figure 6, several examples of the function $X(\theta)$ on the real axis of θ are plotted for different values of x. The function is typically bell-shaped. As x becomes large negative, the width of the support of the bell as well as its height grows proportionally to $-x$. No plateau typical for perturbed rational CFTs is developed. Few samples of $T(\theta)$ (which is the same as $\tilde{T}(\theta)$ at the self-dual point) are presented in figure 7. At x negative and large enough, T develops a plateau in the 'central region' $x < \theta < -x$ of the height which slowly approaches to 2 as $-x$ grows. We will comment more about this approach below. Outside the central region, it starts to oscillate with growing amplitude and frequency. The approach to the asymptotic (4.7) is very fast.

Due to the symmetry $T(\theta) = T(-\theta)$, this function is real on the imaginary axis too. A couple of examples are plotted in figure 8. At x essentially negative, when the plateau is well developed in the central region, the mean value T_0 (see equation (4.9)) is very close to the plateau height, the oscillations around (determined mainly by T_1) being very small ($T_1 \sim R^4$, see equation (8.9)).

The function $T(\theta)$ is real also at the half-period line $\mathrm{Im}\,\theta = \pi/4$. Again, there is a plateau region (at large negative x) of the same height as on the real axis. Then, $T(\theta + \mathrm{i}\pi/4)$ remains positive and grows following the asymptotic (4.8) (see figure 9). Numerical computations in the whole period strip $0 \leqslant \mathrm{Im}\,\theta < \pi/2$ show no sign of other zeros than those on the real axis.

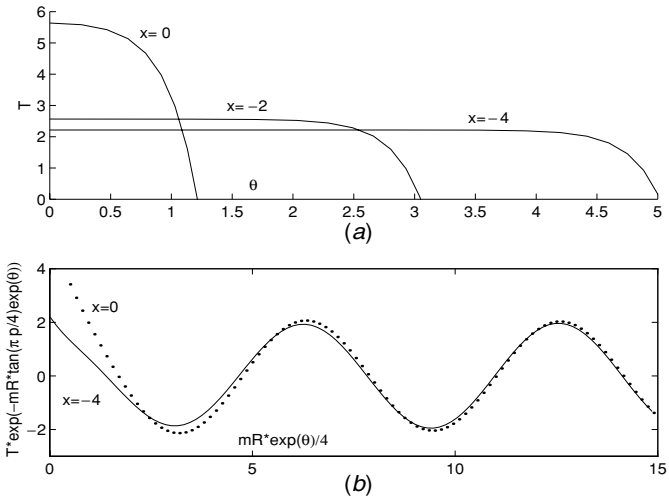

Figure 7. Function $T(\theta)$ on the real axis ($b^2 = 1$).

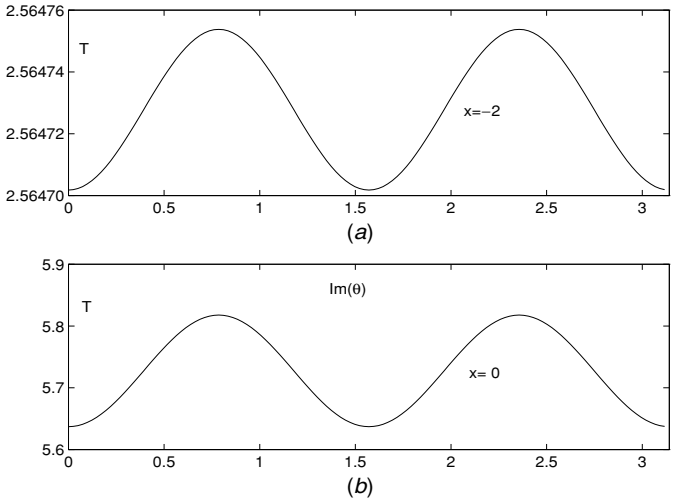

Figure 8. Function $T(\theta)$ along the imaginary axis ($b^2 = 1$).

In figure 10, few examples of $|X(\theta)|$ in the complex plane at different values of $\mathrm{Re}\,\theta$ are plotted versus $\mathrm{Im}\,\theta$ (for $x = 0$). The specific values $\mathrm{Re}\,\theta = 1.22$ and $\mathrm{Re}\,\theta = 2.25$ are chosen close to the positions of the first two zeros of $T(\theta)$ on the real axis. The deeps near $\mathrm{Im}\,\theta = \pi$ and $\mathrm{Im}\,\theta = 3\pi/2$ indicate a presence of zeros of $X(\theta)$ nearby.

More precise positions of zeros of $X(\theta)$ near the line $\mathrm{Im}\,\theta = \pi$ (for the same value $x = 0$) are exemplified in figure 11. In fact, all these zeros are inside the strip $|\mathrm{Im}\,\theta| < \pi$. Only the first zero deviates notably from the line $\mathrm{Im}\,\theta = \pi$. The imaginary parts of next zeros are already very close to π and tend to this value very fast.

7.2. Rational points

As an example of a rational point, we take the simplest case $b^2 = 1/2$. The periods of $T(\theta)$ and $\tilde{T}(\theta)$ are commensurable and equal to $2\mathrm{i}\pi/3$ and $\mathrm{i}\pi/3$, respectively. In fact, in this case,

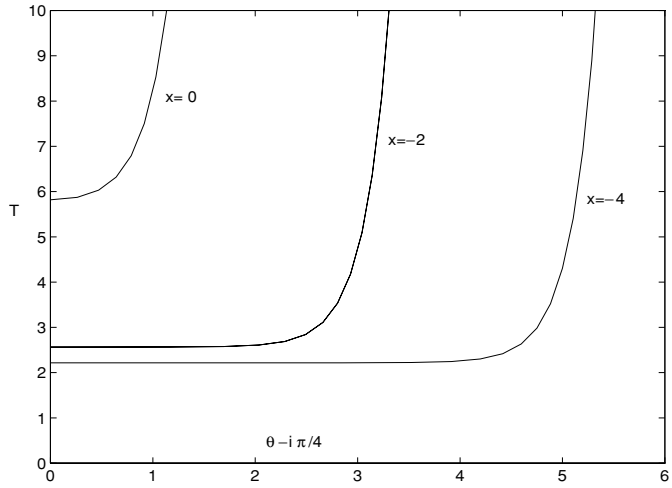

Figure 9. Half-period ($i\pi/4$) shifted $T(\theta)$ at the self-dual point $b^2 = 1$.

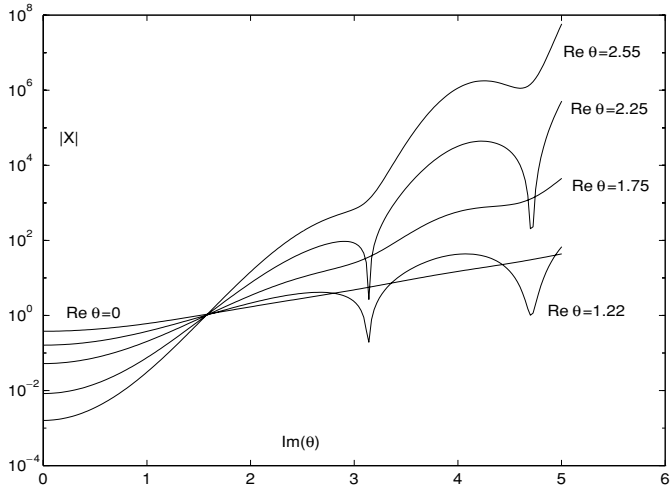

Figure 10. $|X(\theta)|$ as a function of $\mathrm{Im}\,\theta$ at different values of $\mathrm{Re}\,\theta$ ($b^2 = 1$ and $x = 0$).

there is no need to study separately T and $\tilde{T}$ since, as is readily derived from (2.13), they are bound up by the relation

$$\tilde{T}(\theta) = T(\theta)T(\theta + i\pi/3) - 2. \tag{7.1}$$

It should be noted that similar finite degree functional relations between T and $\tilde{T}$ exist for any rational b^2. For example, at $b^2 = 1/3$ the periods of T and $\tilde{T}$ are $3i\pi/4$ and $i\pi/4$ respectively and

$$\tilde{T}(\theta) = T(\theta)T(\theta + i\pi/4)T(\theta + i\pi/2) - T(\theta) - T(\theta + i\pi/4) - T(\theta + i\pi/2). \tag{7.2}$$

Numerical patterns of $T(\theta)$, $\tilde{T}(\theta)$ and $X(\theta)$ are essentially the same as for $b^2 = 1$. I will only show few plots of $|X(\theta)|$ in the complex plane along the lines $\mathrm{Im}\,\theta = \pi, 4\pi/3, 5\pi/3, 2\pi, 7\pi/3$, etc to illustrate the mechanism of multiplication of the zeros' density in the asymptotics $\mathrm{Re}\,\theta \to \infty$ as required by the prediction of figure 2. In figure 12, $|X(\theta)|$

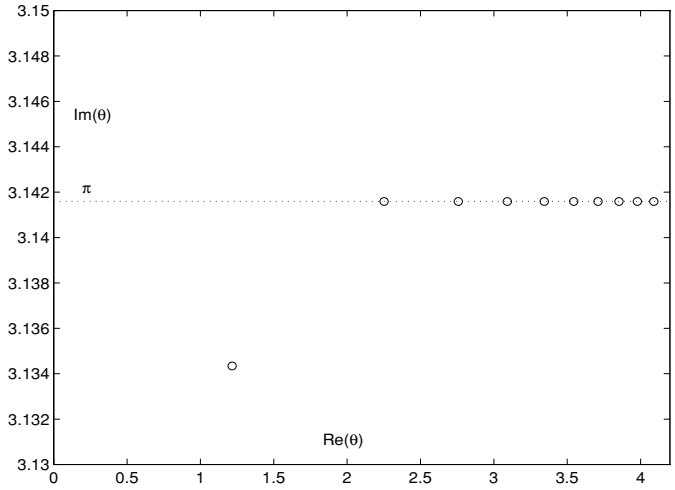

Figure 11. First ten zeros of $X(\theta)$ located near the line $\mathrm{Im}\,\theta = \pi$. An example for $x = 0$ and $b^2 = 1$.

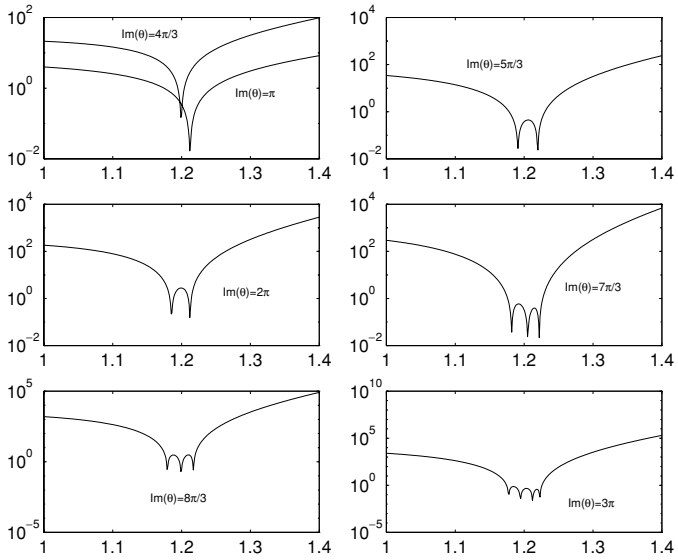

Figure 12. $|X(\theta)|$ versus $\mathrm{Re}\,\theta$ in the vicinity of the first (multi-) zero at $\mathrm{Re}\,\theta \approx 1.2$ and different $\mathrm{Im}\,\theta$ ($x = 0$, $b^2 = 1/2$).

is plotted at $\mathrm{Re}\,\theta$ in the vicinity of the real position of the first zero in $T(\theta)$ at $\theta = 1.2241\ldots$ (the case $x = 0$ is taken as an example). At $\mathrm{Im}\,\theta = \pi$ and $4\pi/3$, the picture indicates simple zeros located closely to this point in $\mathrm{Re}\,\theta$ and slightly displaced in the imaginary direction. At $\mathrm{Im}\,\theta = 5\pi/3$ and 2π, the zeros are split into two closely located ones again near the same position in the real direction. For $\mathrm{Im}\,\theta = 7\pi/3$ and $8\pi/3$, there are triplets of close zeros. In figure 13, the same is exemplified near the next zero of $T(\theta)$ at $\theta = 2.2527\ldots$. It is already seen that the scale of splitting becomes very small with $\mathrm{Re}\,\theta$ growing and such zero multiplets look like multiple zeros if the numerical resolution is not enough.

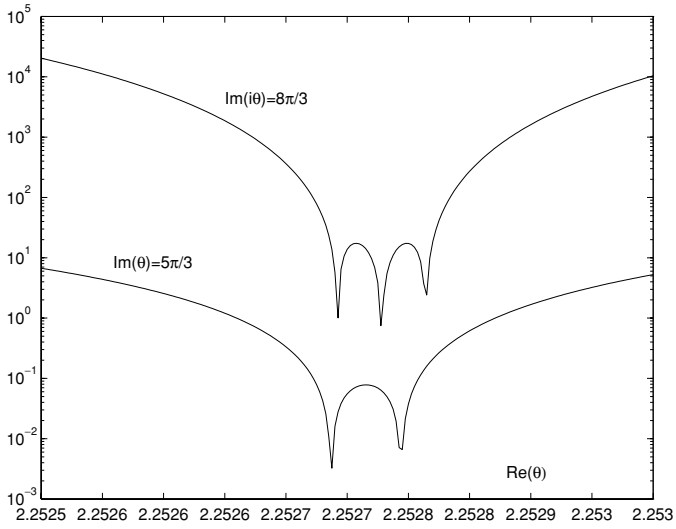

Figure 13. The same as in figure 12 near the next multi-zero at $\mathrm{Re}\,\theta \approx 2.2527\ldots$.

7.3. General real b^2

In general, the periods of $T(\theta)$ and $\tilde{T}(\theta)$ are incommensurable. As was mentioned in section 5, it leads in particular to quite complicated $\mathrm{Re}\,\theta \to \infty$ asymptotics at sufficiently large $\mathrm{Im}\,\theta$. While the analytic structure of $T(\theta)$ and $\tilde{T}(\theta)$ remains essentially as described above (in particular, I verified for many examples that all zeros of T and $\tilde{T}$ are on the real axis), the structure of zeros in $X(\theta)$ becomes, as $\mathrm{Im}\,\theta$ comes essentially large, rather chaotic. I hope to turn again to this point in future studies. Let me mention only the following observation concerning the small R (or large negative x) picture. If $-x \gg 1$, in the central region $x < \theta < -x$ the function $X(\theta)$ matches extremely well the following expression:

$$X(\theta) = \frac{\cos(2QP\theta)}{[\sinh(2\pi bP)\sinh(2\pi P/b)]^{1/2}}, \tag{7.3}$$

where P is an R-dependent parameter. Roughly, it can be estimated from the requirement that $X(\theta) \simeq 0$ at $\theta = \pm x$, i.e. $P = \pi/(-4Qx) + O(x^{-2})$. Note that substituting this approximation in the expression of the effective central charge

$$c_{\mathrm{eff}} = 1 - 24P^2 \tag{7.4}$$

(see [16] for the motivations), we arrive just at the leading UV logarithmic correction (2.16). It is easy to verify that expression (7.3) *satisfies exactly* the functional X system (2.13). This means, in particular, that it remains a valid approximation (at large $-x$) of $X(\theta)$ in the whole complex strip $x < \mathrm{Re}\,\theta < -x$.

In fact along the lines of [16] and [17], a far better estimate of P can be found which takes into account all logarithmic in R corrections to (2.16). In this framework, P is determined as the first root of the transcendental equation

$$4QP\log(R/2\pi) + \mathrm{i}\log(-S_L(P)) = -\pi, \tag{7.5}$$

where $S_L(P)$ is the so-called Liouville reflection amplitude (for the arguments see [16]):

$$S_L(P) = -\left(\pi\mu\frac{\Gamma(b^2)}{\Gamma(1-b^2)}\right)^{-2\mathrm{i}P/b}\frac{\Gamma(1+2\mathrm{i}bP)\Gamma(1+2\mathrm{i}P/b)}{\Gamma(1-2\mathrm{i}bP)\Gamma(1-2\mathrm{i}P/b)}. \tag{7.6}$$

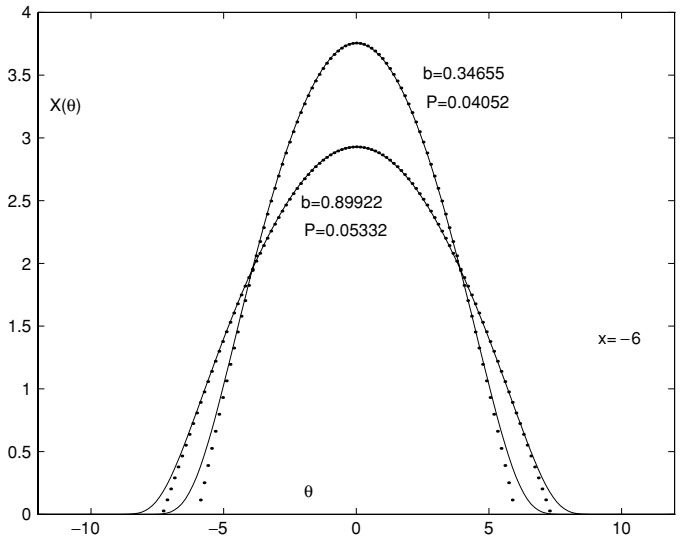

Figure 14. Function $X(\theta)$ at $x = -6$ and different values of b^2 (solid lines) compared with approximation (7.3). Corresponding values of P are indicated.

For example, in figure 14, the shape of $X(\theta)$ is compared with approximation (7.3) for $x = -6$ and two values of the parameter $b^2 = 0.8086\ldots$ and $b^2 = 0.1201\ldots$. According to (7.6), they correspond to $P = 0.053\,32\ldots$ and $P = 0.040\,52\ldots$ respectively.

In view of (7.3), the plateau heights of $T(\theta)$ and $\tilde{T}(\theta)$ in the central region $x < \theta < -x$ and $x \to -\infty$ can be estimated as

$$T_0 = 2\cosh(2\pi b P), \qquad \tilde{T}_0 = 2\cosh(2\pi P/b), \tag{7.7}$$

with the same P determined by (7.6).

7.4. Complex (staircase) values of b^2

The staircase version of the TBA equation (2.3) (with the kernel (6.3)) is solved numerically in the same way as in the ShG case. The structure of the solution has some interesting differences from the case of real b. The peculiarities are more manifested if the parameter θ_0 in (6.3) is taken sufficiently large and the deep UV region $-x \gg 1$ is considered. At $\theta_0 \gg 1$, the parameter b is close to imaginary unity and

$$Q = \frac{\pi}{\sqrt{\theta_0^2 + \pi^2/4}} \tag{7.8}$$

is small.

In figure 15, two pictures of $X(\theta)$ on the real axis are plotted for $x = -46$ and $x = -91$, both at $\theta_0 = 20$. The characteristic staircase behaviour (in fact very similar to that of $Y(\theta)$ observed in [10]) is very apparent. It is also seen that expression (7.3) with the parameter P determined as the solution to the staircase version of (7.5) (in the present case, $P = 0.066\,80\ldots$ and $P = 0.041\,76\ldots$) still follows in the central region the average behaviour of the solution. The deviations (or, in other words, the corrections to approximation (7.3)) are now oscillating and much bigger than those in the ShG case. At sufficiently large $-x$ (many amounts of θ_0), the ascending part (starting from $\theta = x - \theta_0$) of the staircase consists of a succession of almost flat steps of constant width θ_0, the heights being very well fitted by the expression

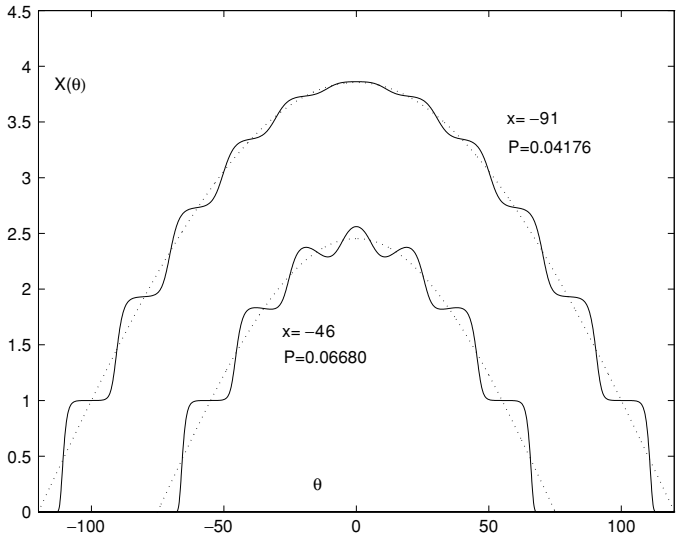

Figure 15. Staircase function $X(\theta)$ at real θ compared with the approximation (7.3) ($\theta_0 = 20$).

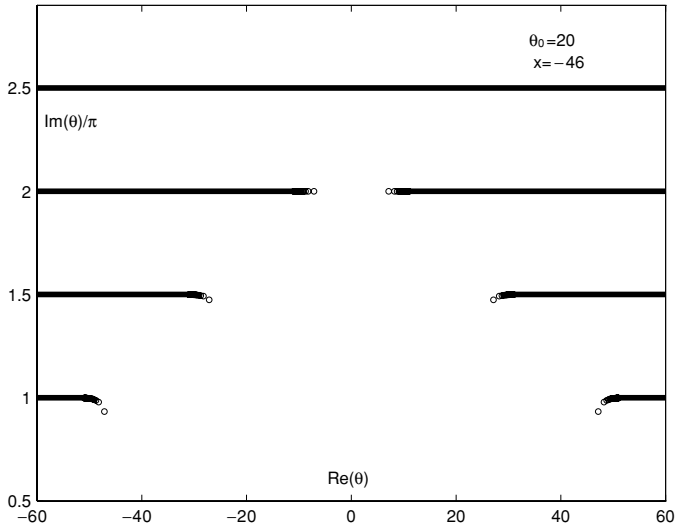

Figure 16. Zeros of $X(\theta)$ at $\theta_0 = 20$ and $x = -46$. Solid lines stand for very dense sets of zeros.

$$X_n = \frac{\sin(2QPn/\theta_0)}{\sin(2QP/\theta_0)}, \tag{7.9}$$

with $n = 0, 1, 2, \ldots$. It should be noted that for the reasons to be explained just below, in the case of complex b, expression (7.3) does not give an approximation in the whole strip $x < \mathrm{Re}\,\theta < -x$. Although (7.3) is still an exact solution to the staircase X system (6.6), its validity is restricted to a certain parallelogram in the complex θ plane.

To see this in figure 16, I present the location of zeros of the function $X(\theta)$ (at $\theta_0 = 20$ and $x = -46$) in the upper half-plane. The picture is obviously reflected in the lower half-plane by the symmetry of $X(\theta)$. We see several strings of zeros accumulating along the

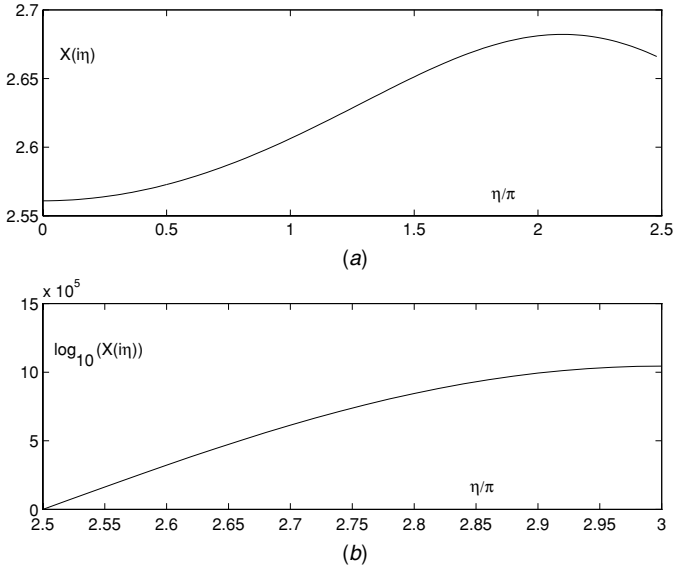

Figure 17. $X(\theta)$ along the imaginary axis ($\theta_0 = 20$, $x = -46$). Plot (b) is in the decilogarithmic scale.

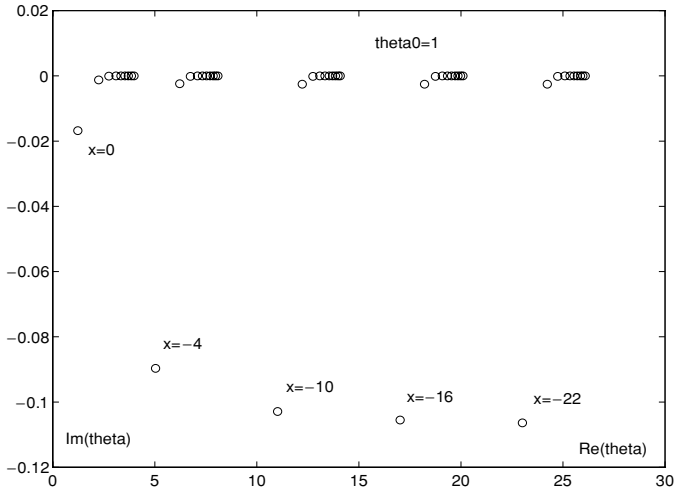

Figure 18. Zeros of $T(\theta)$ at $\theta_0 = 1$ and different x.

lines $\operatorname{Im}\theta = \pi n/2, n = 2, 3, 4, \ldots$, which start at the values $\operatorname{Re}\theta_2 = 47.1500\ldots, \operatorname{Re}\theta_3 = 27.122\,67\ldots \approx \operatorname{Re}\theta_2 - \theta_0, \operatorname{Re}\theta_4 = 7.117\,42\ldots \approx \operatorname{Re}\theta_3 - \theta_0$, etc. There are opposite sets of strings symmetric with respect to the imaginary axis. As n grows, they are shifted in steps of $-\theta_0$ and θ_0 respectively and meet each other at a certain value of n ($n = 5$ in the present example). After that, continuous lines of dense zeros extending from $-\infty$ to ∞ are formed. In general, at large θ_0, the first such line is already dense enough to produce the effect of a 'cut' where the behaviour of $X(\theta)$ changes drastically. In our example, across the first 'cut' at $\operatorname{Im}\theta = 5\pi/2$, the absolute value of $X(\theta)$ jumps by many (10^5) orders of magnitude. This is exemplified in figure 17 where $X(\theta)$ is plotted along the imaginary axis. Note that

before $\mathrm{Im}\,\theta = 5\pi/2$, the function $X(\theta)$ is almost constant. As θ_0 grows, this effect becomes more and more dramatic and in the limit $\theta_0 \to \infty$ the lines of zeros become real cuts. In the forthcoming paper [18], I am going to comment more on this effect which plays a crucial role in the analytic connection between the staircase behaviour at finite θ_0 and the 'sine-Gordon' solutions corresponding to purely imaginary $b = \mathrm{i}\beta$.

In figure 18, the location of zeros of the periodic function $T(\theta)$ is shown at the 'moderate' value $\theta_0 = 1$ and different x. The picture is presented here just to demonstrate two observations: (a) at staircase values of b, zeros of $T(\theta)$ are not exactly on the real axis but displaced slightly to the complex plane, the displacement becoming negligible very quickly with the number of zero, and (b) at $x \to -\infty$, the picture of zeros is 'frozen' in the sense that at x sufficiently large the pattern of zeros is simply shifted by the amount Δx in the θ plane as one changes $x \to x - \Delta x$. As is usual in the TBA practice, it is convenient to study these frozen limiting patterns substituting the original 'massive' TBA equation (2.3) by the massless version of it. This is one of the motivations for the subsequent study (to be published [18]).

8. Concluding remarks

In the present study, I did not touch at all the important question about the R (or x) dependence of the effective central charge (2.2) determined through the finite-size ground state energy (2.1). The UV behaviour at $x \to -\infty$ is especially interesting since the analytic structure of $c_{\mathrm{eff}}(R)$ is quite unusual (like in (2.16)). The Liouville quantization condition (7.5) together with (7.4) proves to be a very good approximation to the UV effective central charge behaviour. However, while it takes into account all the 'soft' (logarithmic in R) contributions to the asymptotic, there are certainly power-like corrections in R. The most important of them (at least at real b) is the contribution of the ground state energy (1.9). Approximation (7.4) is essentially improved if it is taken into account:

$$c_{\mathrm{eff}} = 1 - 24P^2 + 3(mR)^2/(4\pi \sin \pi p). \tag{8.1}$$

Usually, after the ground state energy contribution is subtracted the reminder is a series in the perturbative powers of R like in (2.15). In our present case, with the Lagrangian (1.1) naively one could expect a series like

$$c_{\mathrm{eff}} - 3(mR)^2/(4\pi \sin \pi p) = 1 - 24P^2 + \sum_{n=1}^{\infty} c_n(P)\left(\mu R^{2+2b^2}\right)^{2n}, \tag{8.2}$$

where the powers of R are predicted on dimensional arguments and the coefficients $c_n(P)$ are something like the Coulomb gas perturbative integrals corresponding to the expansion in μ around the vacuum of momentum P (therefore, they keep some smooth R dependence). Although the leading correction $n = 1$ of order R^{4+4b^2} is likely in agreement with the numerical data (at least at sufficiently small b^2), the whole structure (8.2) certainly contradicts duality. The correct expansion must also contain the 'dual' corrections with powers R^{4+4/b^2}. Of course, many people immediately propose to add the dual interaction to the Lagrangian and consider an action like

$$A_{\mathrm{trivial}} = \int \left[\frac{1}{4\pi}(\partial_a \phi)^2 + 2\mu \cosh(2b\phi) + 2\tilde{\mu} \cosh(2b^{-1}\phi)\right] \mathrm{d}^2 x, \tag{8.3}$$

with $\tilde{\mu}$ taken from (1.8) or sometimes introduced as an independent coupling. Simultaneous expansion in both couplings would supposedly lead to a self-dual series

$$c_{\mathrm{eff}} - 3(mR)^2/(4\pi \sin \pi p) = 1 - 24P^2 + \sum_{m,n=1}^{\infty} c_{m,n}(P)\mu^{2m}\tilde{\mu}^{2n} R^{4Q(mb+n/b)}. \tag{8.4}$$

Coefficients $c_{m,n}(P)$ are computed as the mixed Coulomb gas integrals which include both kinds of charges produced by the expansion of action (8.3). Although the general structure of (8.4) looks very likely, to my sense this scenario (which I call trivial) with a naive addition of dual interactions (as in (8.3)) is not exactly in the spirit of duality. However, at present it does not contradict any data and in fact should be verified. A check of this trivial scenario (as well as any other one) requires very subtle measurements of the subleading power-like corrections to the effective central charge as well as tedious calculations of mixed perturbative integrals. I understand that this is a *quantitative* work which can hardly be replaced by general speculations.

Of course, the definition of P as the solution to the quantization condition (7.5) is not completely unambiguous. The power-like corrections in R (which are exponentially small in $1/P$) can be arbitrarily redistributed between the expression for the observable effective central charge (8.4) and the formulation of the quantization condition. In other words, one can add corrections exponentially small in $1/P$ to (7.6) and consider this as a new definition of P. The problem is that at present the parameter P is not precisely observable, i.e. it cannot be directly measured in the TBA calculations (apart from the above-mentioned *definition* through the observable finite-size effective central charge).

At this point, we arrive at the most intriguing question touched only slightly in the present study. This is about the possibility of constructing the solutions $Q_{\pm}(\theta)$ and $\tilde{Q}_{\pm}(\theta)$ of equation (4.12) with properties (4.13) and (4.14) such that the solution to (2.3) can be built as combination (4.15). Had this been possible, we would have another unambiguous definition of the parameter P as the Floquet index in (4.13). However, there are serious doubts that such solutions exist in any sense, at least for rational values of b^2. To clarify this point, in the next publication [18] I will consider the massless version of the ShG TBA equation where the parameter P in introduced from the very beginning instead of the scale parameter R. In this context, solutions (4.13) can be found at least as a formal series for irrational values of b^2 in the way that the construction (4.15) can be given an exact sense.

In connection with the periodic structures encoded in the functions $T(\theta)$ and $\tilde{T}(\theta)$, it seems quite interesting to understand better the R dependence of the coefficients T_n and $\tilde{T}_n$ in expansion (4.9) or (6.9). I checked numerically the $R \to 0$ asymptotic of T_0 and $\tilde{T}_0$. The leading asymptotics of T_0 and $\tilde{T}_0$ (remember that for definiteness in this study, I always take $b \leqslant 1$; in particular, the data discussed in this item were calculated at $b = 0.3466$) are very well fitted by expressions (7.7) with P the solution to (7.5). The correction to (7.7) for T_0 can be set in the form

$$T_0 = 2\cosh(2\pi bP) + (mR/2\pi)^{4bQ} T_0^{(1)}(P), \tag{8.5}$$

where $T_0^{(1)}(P)$ is a smoothly varying function of P with a certain UV limit $T_0^{(1)}(0)$. As for $\tilde{T}_0$, the correction is better fitted as

$$\tilde{T}_0 - 2\cosh(2\pi P/b) \sim A(P)(mR/2\pi)^{\alpha}, \tag{8.6}$$

with α again numerically close to $4bQ$. The common TBA experience would expect from the periodic structure of $\tilde{T}(\theta)$ a much smaller correction $\sim(mR/2\pi)^{4Q/b}$. A probable explanation is that there are some power-like corrections to the Liouville quantization condition (7.5) so that the 'correct' value of P_{correct} is off from P (calculated from (7.5)) by an amount of order $(mR/2\pi)^{4bQ}$

$$P = P_{\text{correct}} + P_{1,0}(mR/2\pi)^{4bQ} + \cdots. \tag{8.7}$$

With this P_{correct}, an asymptotic

$$\tilde{T}_0 = 2\cosh(2\pi P_{\text{correct}}/b) + (mR/2\pi)^{4Q/b}\tilde{T}_0^{(1)}(P_{\text{correct}}) + \cdots \tag{8.8}$$

Table 1. Numerical values of the coefficients (8.10) compared with the CFT predictions (8.11) at $b^2 = 0.346\,5545\ldots$.

x	P	$t_1^1{}_{\rm TBA}$	$t_1^{\rm CFT}$	$\tilde t_1^{\rm TBA}$	$\tilde t_1^{\rm CFT}$
0	0.389 6985	−0.722 8948	−0.721 3854	$-1.452\,134\times10^{-2}$	$-1.437\,650\times10^{-2}$
−2	0.115 2693	−0.658 5087	−0.658 5077	$-8.578\,078\times10^{-3}$	$-8.578\,008\times10^{-3}$
−4	$6.046\,935\times10^{-2}$	−0.654 2746	−0.654 2746	$-8.272\,562\times10^{-3}$	$-8.272\,562\times10^{-3}$

Table 2. The same as in table 1 in the 'staircase' region at $\theta_0 = 10$.

x	P	$t_1^{\rm TBA}$	$t_1^{\rm CFT}$
0	0.177 1863	0.071 1632−1.166 9319i	0.005 1770−1.189 6763i
−15	$8.604\,775\times10^{-2}$	−0.066 0054−0.744 7625i	−0.068 4458−0.744 5886i
−30	$5.695\,833\times10^{-2}$	−0.070 8064−0.656 8688i	−0.070 9316−0.656 8002i

must hold. If the power $4Q/b \gg 4bQ$ (like in the present experiment with $4Q/b = 37.31\ldots \gg 4bQ = 4.480\ldots$), we can even try to relate the coefficient A in (8.6) to the leading power correction to (7.5). As the corrections in (8.8) are much more suppressed at $R \to 0$, this seems reasonable.

It is easy to verify that the leading asymptotics of the higher coefficients T_n and $\tilde T_n$ in expansion (4.9) are of the form

$$\begin{aligned} T_n &= (mR/2\pi)^{2bQ|n|}T_n^{(0)}(P) + \cdots \\ \tilde T_n &= (mR/2\pi)^{2Q|n|/b}\tilde T_n^{(0)}(P) + \cdots, \end{aligned} \tag{8.9}$$

with $T_n^{(0)}(P)$ and $\tilde T_n^{(0)}(P)$ regular at $P = 0$. I analysed quantitatively the functions $T_1^{(0)}(P)$ and $T_1^{(0)}(P)$. Motivated by the constructions of [14, 19], let us introduce slightly rescaled functions

$$t_1(P) = T_1^{(0)}(P)(Z(p))^{-2bQ}, \qquad \tilde t_1(P) = \tilde T_1^{(0)}(P)(Z(p))^{-2Q/b}, \tag{8.10}$$

with $Z(p)$ defined in (1.7). In table 1, the values of $t_1(P)$ and $\tilde t_1(P)$ are compared with the following analytic expressions borrowed from [19, 14] where these coefficients enter the explicit constructions of the 'sine-Gordon' (i.e. related to purely imaginary values of b) analogues of $T(\theta)$,

$$\begin{aligned} t_1^{\rm CFT}(P) &= -\frac{4\pi^2\Gamma(1+2b^2)}{\Gamma^2(b^2)\Gamma(1+b^2+2{\rm i}bP)\Gamma(1+b^2-2{\rm i}bP)}, \\ \tilde t_1^{\rm CFT}(P) &= -\frac{4\pi^2\Gamma(1+2b^{-2})}{\Gamma^2(b^{-2})\Gamma(1+b^{-2}+2{\rm i}P/b)\Gamma(1+b^{-2}-2{\rm i}P/b)}. \end{aligned} \tag{8.11}$$

The TBA numbers are measured at $b = 0.346\,5545\ldots$ and different values of x. The same for the staircase example $\theta_0 = 10$ is presented in table 2. The convergence is notably slower due to much weaker suppression of the higher power corrections ($\mathrm{Re}(4+4b^2) = 0.1926\ldots$ in this case). The numbers quoted make it clear that an analytic continuation of the constructions of [14, 19] for the ShG or staircase values of the parameter is quite relevant. The corresponding 'CFT integrable structures' will be shown to have a precise relation to the solutions of the massless versions of ShG and staircase TBA equations [18] where the parameter $P = P_{\rm correct}$ is fixed by construction.

I would like to mention a quite intriguing recent article [20] where the author arrived at function (2.9) in a rather different context. It appears as the exact wavefunction of the finite-size sinh-Gordon model in special 'γ-coordinates' which are the sinh-Gordon version

of the Flaschka–McLaughlin variables (see [20] for the details). This again gives a motivation to continue the study of the analytic structures related to the ShG TBA equation.

Acknowledgments

I acknowledge very useful discussions with C Ahn, V Bazhanov, V Fateev, C Rim and mostly with A Zamolodchikov. I also thank P Wiegmann who brought my attention to papers [12, 13] and introduced to me the world of incommensurable periods. Discussions with G Mussardo about the 'double sinh-Gordon' [21] were also quite relevant. My special gratitude is to S Lukyanov who communicated me his article [20] before publication and encouraged my work by exciting discussions. The work is supported in part by EU under the contract ERBFMRX CT 960012.

References

[1] Vergeles S and Gryanik V 1976 Two-dimensional quantum field theories having exact solutions *Yad. Fiz.* **23** 1324
Vergeles S and Gryanik V 1976 Two-dimensional quantum field theories having exact solutions *Sov. J. Nucl. Phys.* **23** 704
[2] Arefyeva I and Korepin V 1974 Scattering in two-dimensional model with Langrangian $(1/\gamma)((\partial(\mu)u)^2/2 + m^2\cos(u-1))$ *Pisma Zh. Eksp. Teor. Fiz.* **20** 680
[3] Zamolodchikov Al 1995 Mass scale in sine-Gordon and its reductions *Int. J. Mod. Phys.* A **10** 1125
[4] Destri C and deVega H 1991 New exact results in affine Toda field theories: free energy and wave function renormalizations *Nucl. Phys.* B **358** 251
[5] Lukyanov S and Zamolodchikov A 1997 Exact expectation values of local fields in quantum sine-Gordon model *Nucl. Phys.* B **493** 571
[6] Fateev V, Fradkin D, Lukyanov S, Zamolodchikov A and Zamolodchikov Al 1999 Expectation values of descendent fields in the sine-Gordon model *Nucl. Phys.* B **540** 587
[7] Koubek A and Mussardo G 1993 On the operator content of the sinh-Gordon model *Phys. Lett.* B **311** 193
[8] Zamolodchikov Al 1991 *Phys. Lett.* B **253** 391
[9] Quattrini E, Ravanini F and Tateo R 1993 Integrable QFT(2) encoded in products of Dynkin diagrams *Preprint* hep-th/9311116
[10] Zamolodchikov Al 1991 Resonance factorized scattering and roaming trajectories, ENS-LPS-335 unpublished
[11] Hirota R 1981 *J. Phys. Soc. Japan* **50** 3785
[12] Wiegmann P 1997 Bethe ansatz and classical Hirota equations *Int. J. Mod. Phys.* B **11** 75 (*Preprint* cond-mat/9610132)
[13] Wiegmann P and Zabrodin A 1995 Algebraization of difference eigenvalue equations related to $U_q(sl_2)$ *Nucl. Phys.* B **451** 699 (*Preprint* cond-mat/9501129)
[14] Bazhanov V, Lukyanov S and Zamolodchikov A 1997 Integrable structure of conformal field theory II. Q-operator and DDV equation *Commun. Math. Phys.* **190** 247
[15] Hirota R 1987 *J. Phys. Soc. Japan* **56** 4285
[16] Zamolodchikov A and Zamolodchikov Al 1996 Structure constants and conformal bootstrap in Liouville field theory *Nucl. Phys.* B **477** 577
[17] Ahn C, Fateev V, Kim C, Rim C and Yang B 2000 Reflection amplitudes of ADE Toda theories and thermodynamic Bethe ansatz *Nucl. Phys.* B **656** 210
[18] Zamolodchikov Al Massless sinh-Gordon TBA equations in preparation
[19] Bazhanov V, Lukyanov S and Zamolodchikov A 1996 Integrable structure of conformal field theory, quantum kdV theory and thermodynamic Bethe ansatz *Commun. Math. Phys.* **177** 381
[20] Lukyanov S 2001 Finite temperature expectation values of local fields in the sinh-Gordon model *Nucl. Phys.* B **612** 391 (*Preprint* hep-th/0005027)
[21] Delfino G and Mussardo G 1998 Non-integrable aspects of the multi-frequency sine-gordon *model. Nucl. Phys.* B **516** 675